Molecular Transition and Slip Flows in Rotating Helical Channels of Drag Pump

Young-Kyu Hwang and Joong-Sik Heo

School of Mechanical Engineering, Sungkyunkwan University, 300 Chunchun-dong, Jangan-ku, Suwon 440-746, S. Korea

Abstract. Numerical and experimental investigations are performed for the rarefied gas flows in pumping channels of a helical-type drag pump. Modern turbomolecular pumps include a drag stage in the discharge side, operating roughly in the pressure range of 10^{-2}~10Torr. The flow occurring in the pumping channel develops from the molecular transition to slip flow traveling downstream. Two different numerical methods are used in this analysis: the first one is a continuum approach in solving the Navier-Stokes equations with slip boundary conditions, and the second one is a stochastic particle approach through the use of the direct simulation Monte Carlo (DSMC) method. The flows in pumping channels are three-dimensional (3D), and the main difficulty in modeling a 3D case comes from the rotating frame of reference. Thus, trajectories of particles are no longer straight lines. In the present DSMC method, trajectories of particles are calculated by integrating a system of differential equations including the Coriolis and centrifugal forces. Our study is the first instance to analyze the rarefied gas flows in rotating frame in the presence of noninertial effects.

INTRODUCTION

Today, molecular drag stages are widely used in conjunction with a turbomolecular pump in order to improve the pumping performance of it.[1] For example, compound or hybrid molecular pumps have gained wide attention because of their increased pumping throughput and discharge pressure. The drag pump may be of the Holweck (helical-type) or Siegbahn (disk-type) design. In the present study, the pumping performance of a helical-type drag pump (HTDP) is numerically and experimentally analyzed. The flow within a pumping channel of a HTDP varies from the molecular transition to slip flow regime. Two different numerical methods are used: one is a continuum approach in solving the Navier-Stokes (N-S) equations with slip boundary conditions, and the other is a stochastic particle approach through the use of the direct simulation Monte Carlo (DSMC) method.

Panos *et al.*[2] defined the separation pressure between the viscous and the free molecular state, and they extended Gaede's equation, which was used for the helical single-groove drag pump in the free molecular flow, to the helical multi-groove drag pump in both the viscous and free molecular states. Nanbu *et al.*[3] numerically studied the molecular transition and slip flows in helical channels by using the DSMC method. Sawada[4] analyzed the pumping mechanism by solving the N-S equations with slip boundary conditions. However, the previous studies[2-4] were limited to the quasi three-dimensional (Q3D) model of Couette flow. Namely, the three-dimensional (3D) rotating helical channel was considered as a rectangular groove facing a wall, which is linearly moving along the groove; see Fig. 1.

In the recent study of Niu[5] and Cheng *et al.*[6], the rotating helical channels were three-dimensionally modeled to investigate the curvature effect of channels, and a laminar compressible N-S solver with first-order velocity slip condition was used.

In the present study, the DSMC method using the 3D model is employed to investigate the effect of Coriolis and centrifugal forces on the pumping performance. Also, the formulation of second-order slip boundary conditions (SBC) is utilized in the N-S method. As a validation for our work, the present numerical results for Q3D and 3D models are first compared with the previously known numerical and experimental ones obtained by Nanbu *et al.*[3] Of the two models, the 3D model gives more accurate results than does the Q3D model. Our experimental results are presented in the pressure range of 0.02~4 Torr and are compared with numerical ones for both models. Also, we assess the validity and usefulness of the N-S simulations in the molecular transition regime.

CP585, *Rarefied Gas Dynamics: 22nd International Symposium*, edited by T. J. Bartel and M. A. Gallis

Report Documentation Page

Report Date	Report Type	Dates Covered (from... to)
09JUL2000	N/A	-

Title and Subtitle Molecular Transition and Slip Flows in Rotating Helical Channels of Drag Pump	**Contract Number**
	Grant Number
	Program Element Number
Author(s)	**Project Number**
	Task Number
	Work Unit Number
Performing Organization Name(s) and Address(es) School of Mechanical Engineering, Sungkyunkwan University, 300 Chunchun-dong, Jangan-ku, Suwon 440-746, S. Korea	**Performing Organization Report Number**
Sponsoring/Monitoring Agency Name(s) and Address(es) AOARD Unit 45002 APO AP 96337-5002	**Sponsor/Monitor's Acronym(s)**
	Sponsor/Monitor's Report Number(s)

Distribution/Availability Statement
Approved for public release, distribution unlimited

Supplementary Notes
Papers from Rarefied Gas Dynamics (RGD) 22nd International Symposium held in Sydney, Australia on 9-14 July 2000. See also ADM001341 for whole conference on cd-rom.

Abstract

Subject Terms

Report Classification unclassified	**Classification of this page** unclassified
Classification of Abstract unclassified	**Limitation of Abstract** UU

Number of Pages
7

COMPUTATIONAL MODELS

Two different kinds of helical rotors are illustrated in Figs. 1(a) and 1(b), where α is the helix angle, a the channel width, b the ridge width, d the channel depth, and Δd the clearance between rotor and stator. The Knudsen number is defined as $Kn = \lambda / d$, where λ is the mean free path of molecules. The geometrical dimensions of channels are given in Table 1. The channel depth of rotor 1 is 4 mm, while that of rotor 2 is continuously varied from 8 mm (at inlet) to 4 mm (at outlet). Also, the channel shape of rotor 2 consists of two parts, *i.e.*, $\alpha_1 = 40°$ for the upper part of channels and $\alpha_2 = 15°$ for the lower part of channels, respectively.

Two different numerical methods are used in the present investigation. The first one is the continuum approach, in which the N-S equations with slip boundary conditions are solved numerically. The second one is the molecular approach, in which a direct physical simulation is performed by considering interactive motions of molecules. The DSMC method of Bird[7] is employed to solve the problem of internal rarefied flows in pumping channels. To save space, we do not discuss here the procedures in obtaining solutions of the N-S equations; but we refer the reader to Sawada.[4]

DSMC SIMULATIONS

The simulated physical space is divided into a network of cells. Figures 2(a) and 2(b) illustrate the computational grid of the 3D channel for rotors 1 and 2, respectively. A rectangular grid system is used in Q3D model, as seen in Fig. 3. In the case of 3D model, each cell is subdivided into five tetrahedral subcells, which have four well-defined triangular faces, to enable tracking the molecules from one cell to another.

A large number of molecules is uniformly distributed in the computational domain, and the initial velocities of molecules are evaluated from the Maxwellian distribution function. The gas flows entering the open boundary of the computational domain are initially assumed to be in equilibrium, with zero bulk velocity. The bulk velocity is updated by iteration. If a molecule collides with the wall, a new reflected velocity is assigned by the surface boundary condition. Both wall and gas molecules passing through the pumping channels are assumed to be in an isothermal (300 K) state. In the present simulation, the gas is nitrogen. The null-collision technique of Koura[8] is adopted to determine the number of collision pairs selected within a cell during time step Δt. The collision process is accounted by using the variable soft sphere molecular model of Koura and Matsumoto.[9] The flow field is sampled every 5 time steps during 20000 time steps after reaching the steady state.

TABLE 1. Geometrical dimensions of helical-type rotors

Rotor		**1**	**2**
Rotor diameter	D	168.6 mm	168.6 mm
Rotor axial length	L	132.0 mm	$L_1 = 66.0$ mm
			$L_2 = 66.0$ mm
Helix angle	α	15°	$\alpha_1 = 40°$
			$\alpha_2 = 15°$
Channel width	a	13.6 mm	$a_1 = 42.2$ mm
			$a_2 = 13.6$ mm
Ridge width	b	5.4 mm	$b_1 = 5.4$ mm
			$b_2 = 5.4$ mm
Channel depth	d	4.0 mm	$d_1 = 8.0$ mm
			$d_2 = 4.0$ mm
Clearance	Δd	0.9 mm	0.9 mm
No. of grooves	N_b	7	7
Rotational speed	rpm	24000	24000

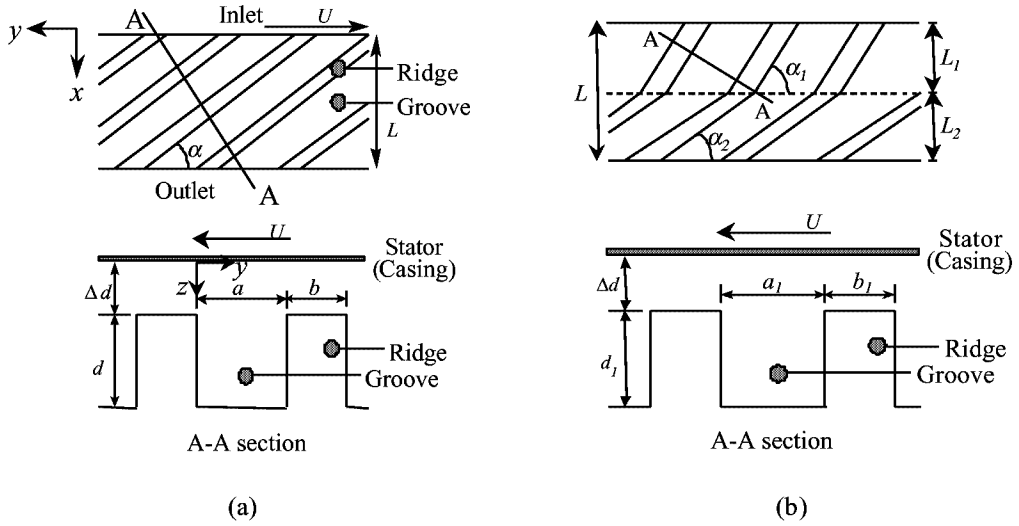

FIGURE 1. Geometry of helical-type drag pump (Q3D): (a) rotor 1; (b) rotor 2.

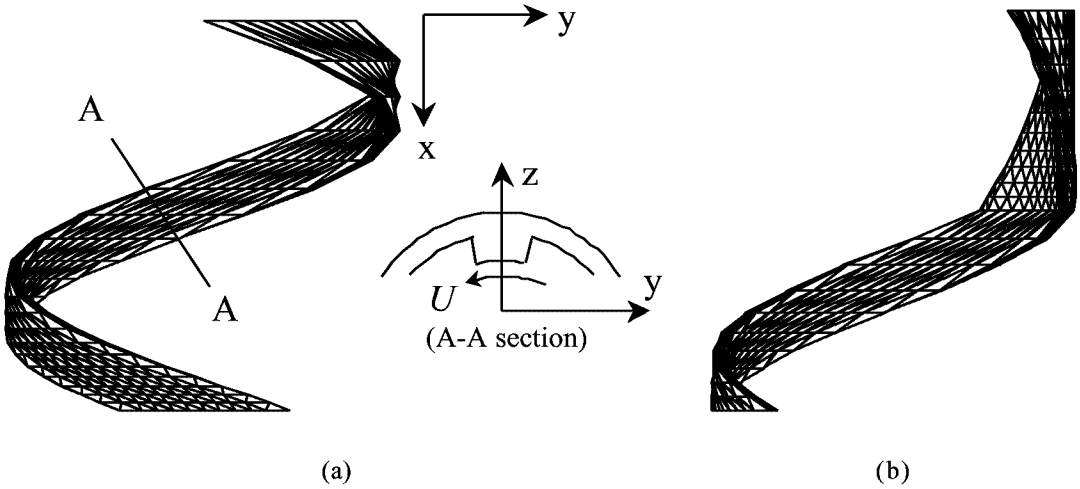

FIGURE 2. Computational grid system for 3D helical channel: (a) rotor 1; (b) rotor 2.

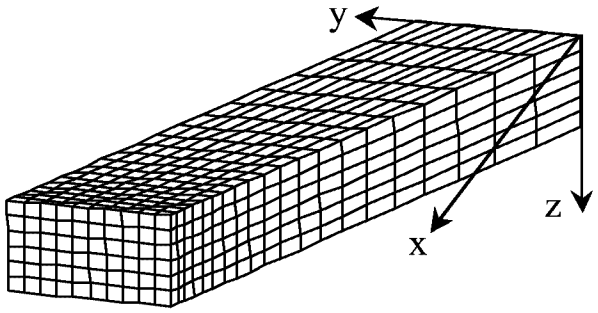

FIGURE 3. Computational grid system for Q3D model (rotor 1).

The main difficulty in modeling a 3D case comes from the rotating frame of reference. In particular, trajectories of particles are not straight lines in the rotating frame. Thus, trajectories are calculated by integrating a system of differential equations, including the Coriolis and centrifugal forces. The fourth-order Runge-Kutta algorithm is used to integrate the following equation:

$$a_r = -\omega \times (\omega \times r_{mol}) - 2\omega \times V_{mol}, \tag{1}$$

in which a_r is the relative acceleration, r_{mol} and V_{mol} is the trajectory and the relative velocity of molecules, and ω is the angular velocity of the rotor.

From Eq. (1) we can find positions and velocities of particles at any time on the $y-z$ plane; see Fig. 2(a). The component of the particle velocity along the $x-$axis, c_x, is independent of the frame of reference, *i.e.*, c_x is the same for both moving and nonmoving frames of reference.

At the end of the simulation, the dimensionless pumping efficiency w, pumping speed S (l/s), and throughput Q ($Torr \cdot l/s$) are calculated by

$$w = \frac{N_{12} - N_{21}}{N_{inlet}}, \tag{2}$$

$$S = w \cdot A_1 \cdot \sqrt{8RT/\pi} \cdot K(s_1)/4.0, \tag{3}$$

where

$$K(s_1) = \exp(-s_1^2) + \sqrt{\pi} s_1 [1.0 + erf(s_1)], \; s_1 = u_1 / \sqrt{2RT},$$

and

$$Q = P_1 \cdot S, \tag{4}$$

in which N_{12} (or N_{21}) is the number of particles to be transmitted through the channel from the inlet (or outlet) to the outlet (or inlet), and N_{inlet} is the number of particles coming from the inlet during sampling time.[3] The quantity u_1 is the x component of the bulk velocity crossing the open boundary.

EXPERIMENTAL APPARATUS

To verify the present numerical results, experiments on the pumping characteristics of a HTDP are carried out by using the test pump. Dimensions of the helical-grooved rotor of the test pump are listed in Table 1. The rotor is 168.6 mm in diameter and 132 mm in axial length. It has seven threaded rectangular grooves.

A schematic diagram of the experimental apparatus is shown in Fig. 4. This apparatus mainly consists of two parts: the test pump, and instruments that facilitate pressure measurements and flow supply into the test pump. The test pump is connected to a two-stage oil rotary pump (970 *l/min*). The pressure in the high-vacuum side is measured with a Pirani (7.6×10^{-4}~ 7.6 Torr) and Penning (7.6×10^{-8}~ 7.6×10^{-3} Torr) gauge, and the pressure in the fore-vacuum side is measured with a Pirani gauge.

Experiments are performed by varying the outlet pressure P_2 in the range of 0.02 Torr $\leq P_2 \leq$ 4 Torr. The rotational speed of the rotor is 24,000 rpm and is controlled by a frequency converter. Test gas (N_2) is supplied through a mass flow controller from a regulated high-pressure cylinder.

RESULTS AND DISCUSSION

The present numerical results are compared with the previously known numerical and experimental ones obtained by Nanbu *et al.*[3], as shown in Fig. 5. The computations are conducted by employing the DSMC and N-S

methods by changing the inlet pressure P_1 for the fixed outlet pressure P_2 = 0.3 Torr. The present DSMC results for Q3D model agree well with those of Nanbu *et al.* But the N-S results deviate from those of the DSMC method. The throughput Q increases linearly as the pressure difference ΔP ($= P_2 - P_1$) decreases. The DSMC results for Q3D model underestimate by as much as 20% in the throughput at ΔP = 0.1 Torr compared to the experimental data. This discrepancy is partly related to a motion between the rotor and casing wall, which is assumed to be linear in Q3D model.

Also, the DSMC results for 3D model are shown in Fig. 5. In the case of Q3D model, only the moving effect of the casing wall on the performance exists; however, in the 3D model, Coriolis and centrifugal forces are dominant effects along with the curvature of channels. In the present study, these effects on the pumping performance are considered. Consequently, it is seen that the DSMC results which employ 3D model give the best correspondence to the experimental data.

The variations of P_1 as a function of Q at P_2 = 0.8 and 1.0 Torr are shown in Figs. 6 and 7 for rotors 1 and 2, respectively. The value of P_1 becomes higher as Q increases, and it depends on P_2. Comparison between the experimental data and the DSMC results shows good agreement.

The effect of the outlet pressure on the inlet pressure at zero-flow condition is shown in Fig. 8 for rotor 1, and the comparison between the experimental data and the numerical results is also made. Comparison between the experimental data and the N-S results shows good agreement in the range of $P_2 \geq 2$ Torr (in this region, $Kn = \lambda_2 / d$, based on the mean free path λ_2 at the outlet and the channel depth d, is in the order of 10^{-3}). But the discrepancy between the two results becomes larger for $P_2 \leq 1.14$ Torr, *i.e.*, $Kn \geq 0.01$. This indicates that the slip flow analysis of the N-S method is inappropriate for $Kn \geq 0.01$.

In the slip flow regime, it has generally been recognized that the layer of gas adjacent to the wall is no longer at rest but has a finite slip velocity. Thus the continuum assumption is not valid near the wall. From the momentum transfer between gas and wall, the slip on the wall surfaces is given by:

$$u_s = u_w + \frac{2-\sigma}{\sigma} Kn \left(\frac{\partial u}{\partial n} \right)_w , \tag{5}$$

where σ is the accommodation coefficient, u_s and u_w refer to the slip velocity and the wall velocity, respectively.

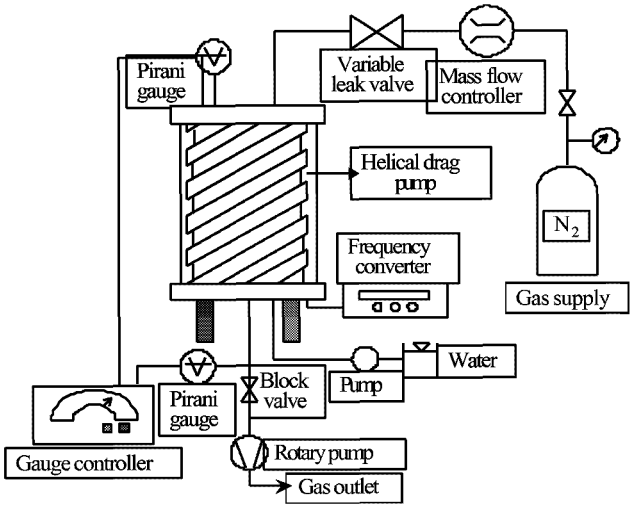

FIGURE 4. Schematic diagram of experimental apparatus.

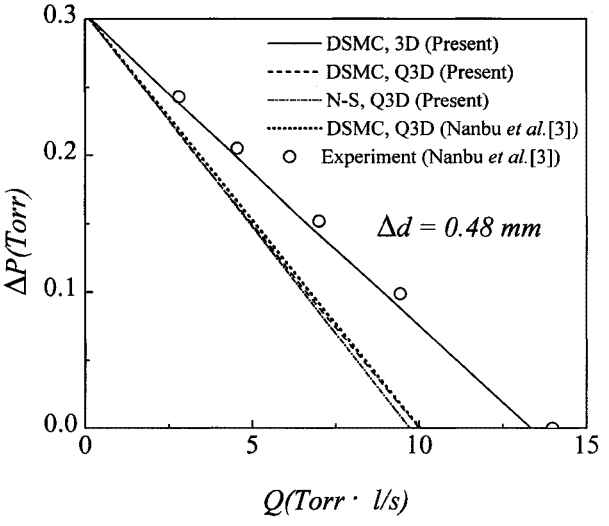

FIGURE 5. Performance curves at P_2=0.3 Torr.

In the above, n is the non-dimensional coordinate perpendicular to the channel wall that is normalized by the channel depth d, and subscript w indicates that the variable is evaluated at the wall.

The boundary condition of Eq. (5) is viewed as an expansion of the velocity gradient at the wall in powers of Kn. For continuum flow, $Kn \to 0$, Eq. (6) reduces to the familiar no-slip condition. Specifically, the no-slip condition and Eq. (5) are the zeroth and the first-order approximations, respectively. For the second-order modification, the following slip velocity can be utilized in the case of $\sigma = 1$:

$$u_s = u_w + Kn\left(\frac{\partial u}{\partial n}\right)_w + \frac{Kn^2}{2}\left(\frac{\partial^2 u}{\partial n^2}\right)_w . \tag{6}$$

As seen in Fig. 8, the results obtained by the N-S method with second-order SBC are nearly the same as those with first-order SBC in the range of $P_2 > 1$ Torr. The differences between the two results appear noticeably for $P_2 <$ 0.1 Torr. Although the N-S method with second-order SBC fails to predict quantitatively the experimental data, it seems that the results obtained by second-order SBC agree qualitatively with the experimental data compared to those obtained by first-order SBC.

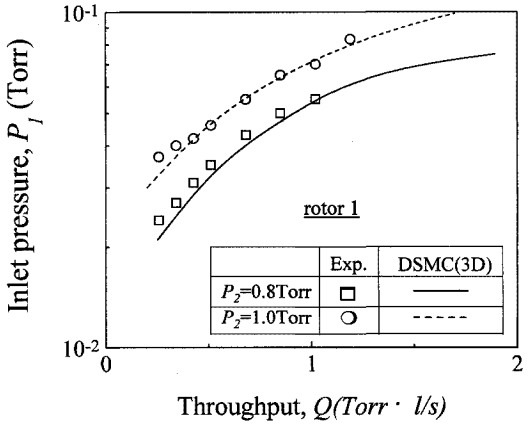

FIGURE 6. Inlet pressure *vs.* throughput of rotor 1.

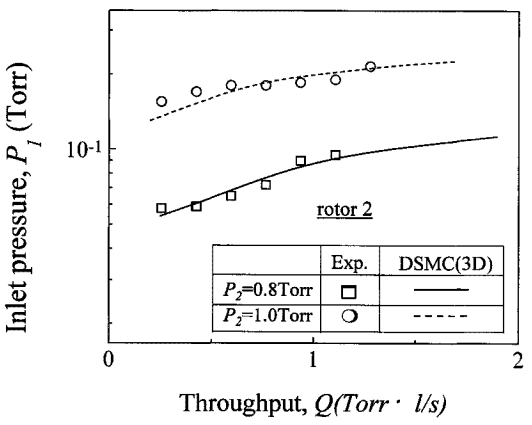

FIGURE 7. Inlet pressure *vs.* throughput of rotor 2.

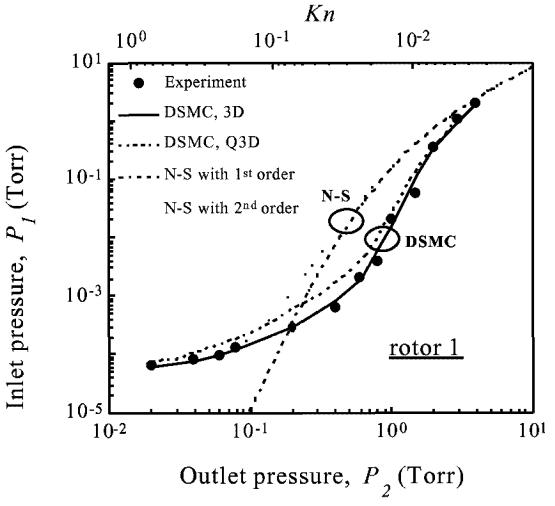

FIGURE 8. Inlet pressure *vs.* outlet pressure.

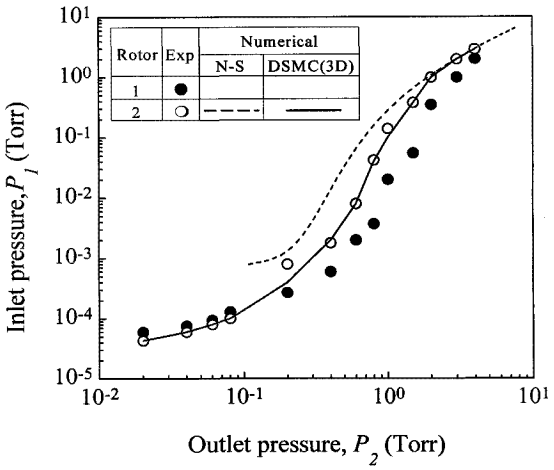

FIGURE 9. Performance comparison of rotor 1 with rotor 2.

Experimental results are also compared with those obtained by the DSMC simulations. The good agreement between the two is shown in Fig. 8. This clearly reveals the ability of the DSMC method to predict the molecular transition flows. Especially, the 3D model predicts well the experimental data compared to the Q3D model.

In general, the computing cost of the DSMC simulation is linearly proportional to the gas density and the size of a computational cell, which should be scaled with the mean free path. Therefore, a high density flow requires a large number of computational cells. This means that more particles and more collisions between molecules must be accounted for in the computation. Consequently, for $10^{-2} \leq Kn \leq 1$, although the DSMC method provides more accurate solutions than does the N-S method, it requires much more computational effort and higher expenses as Kn decreases.

The effect of the outlet pressure on the inlet pressure at zero-flow condition for rotor 2 is shown in Fig. 9. For comparison, the experimental data for rotor 1 in Fig. 8 are also included in this figure. The N-S results presented here are those obtained by the second-order method. It is seen that the maximum attainable inlet pressure is about 6×10^{-5} Torr for rotor 1 and 4.3×10^{-5} Torr for rotor 2, respectively. As indicated in Fig. 8 for rotor 1, the N-S results for rotor 2 also deviate from the experimental data, except the range of $P_2 \geq 2$ Torr. On the other hand, as expected, the DSMC results give good correspondence to the experimental data.

CONCLUDING REMARKS

Numerical and experimental studies have been made for the molecular transition and slip flows in the rotating helical channel of a HTDP. The computations are conducted by employing the N-S and DSMC methods. Experiments were performed by varying the outlet pressure P_2 in the range of 0.02 Torr $\leq P_2 \leq$ 4 Torr.

A new 3D model of a helical channel has been developed, and the effects of the Coriolis and centrifugal forces on the pumping performance are discussed. The numerical results indicate that the present 3D model gives more accurate solutions than does the previous Q3D model.

Also, the present results obtained by the N-S and DSMC methods agree well with the experimental data for $Kn \leq 0.01$. In particular, the N-S method with SBC drastically simplifies the simulation and saves computational effort in predicting the performance for this regime.

ACKNOWLEDGMENT

This work was supported by the Brain Korea 21 Project.

REFERENCES

1. Hablanian, M. H., in *Vacuum Science and Technology: Pioneers of 20th Century*, AIP, New York, 1994.
2. Panos, C. N., Antoniou, A. G. and Valamontes, S. E., "The Helicoid Multi-Groove Vacuum Pump in Both Viscous and Molecular States," *Vacuum*, Vol. 45, No. 8, 1994, pp. 841-847.
3. Nanbu, K., Kubota, H., Igarashi, S., Urano, C. and Enosawa, H., "Performance of Spiral Grooves on a Rotor of Turbo-molecular Pump," *Trans. JSME*, Vol. 57, No. 533, 1991, pp. 172-177.
4. Sawada, T., "Rarefied Gas Flow in a Rectangular Groove Facing a Moving Wall," *Sci. Papers of IPCR*, Vol. 70, No. 4, 1976, pp. 79-86.
5. Niu, Y. Y., "Navier-Stokes Analysis of Gaseous Slip Flow in Long Grooves," *Numerical Heat Transfer: Part A*, Vol. 36, No. 1, 1999, pp. 75-93.
6. Cheng, H. P., Jou, R. Y., Chen, F. Z., Chang, Y. W., Iwane, M. and Hanaoka, T, "Three-Dimensional Flow Analysis of Spiral-Grooved Turbo Booster Pump in Slip and Continuum Flow," *J. Vac. Sci. Technol. A*, Vol. 18, No. 2, 2000, pp. 543-551.
7. Bird, G. A., *Molecular Gas Dynamics and the Direct Simulation of Gas Flows*, Clarendon Press, Oxford, 1994.
8. Koura, K., "Null-collision Technique in the Direct Simulation Monte Carlo Method," *Phys. Fluids*, Vol. 29, No. 11, 1986, pp. 3509-3511.
9. Koura, K. and Matsumoto, H., "Variable Soft Sphere Molecular Model for Air Species," *Phys. Fluids*, Vol. 4, No. 5, 1992, pp. 1083-1085.